LAWRENCE
LIVERMORE
NATIONAL
LABORATORY

LLNL-TR-608916

Dynamics of the Eagle Nebula

M. Pound

December 20, 2012

Disclaimer

This work performed under the auspices of the U.S. Department of Energy by Lawrence Livermore National Laboratory under Contract DE-AC52-07NA27344.

Final Report on NIF Concept Development award B595751, *Dynamics of the Eagle Nebula*

Marc W. Pound
University of Maryland, College Park

August 6, 2012

1 Introduction

The purpose of this study was to investigate some required details of the experimental design needed to field a credible, well-scaled Eagle Nebula HEDLP experiment on NIF. These details were addressed through new astronomical observations and review of existing literature. Below, we list the deliverables as given in the Statement of Work and discuss each in turn.

UMCP Astronomy first-year graduate student Erin Grand was supported by the grant from August 01, 2011 to June 24, 2012 to oversee the CARMA observations, and reduce and analyze the data therefrom. For the remainder of Summer 2012, she is continuing the analysis with support by the CARMA consortium grant. The data, results, and analysis will form the core of her Second-Year Research Project (2YP), required to advance to Ph. D. candidacy in the Astronomy Department. A shorter version of her 2YP report (with less introductory material) will be submitted for publication in a major astronomical journal.

Initial results from this study were presented in a poster by Grand and Pound at the 9th International Conference on High Energy Density Laboratory Astrophysics, held on April 30-May 4, 2012 at Florida State University in Tallahassee, Florida. This poster is attached as Appendix A.

2 Deliverables

1. **CARMA Observing Proposal #1, to investigate dense gas distribution in Eagle and Pelican Nebulae**

   This proposal was submitted to the Combined Array for Research in Millimeter Astronomy (CARMA) Telescope Allocation Committee in April 2011. This successful proposal was subsequently allocated 40 hours to observe several dense molecular gas tracers [HCN(J=1-0), HCO^+(J=1-0), CS(J=2-1), N_2H^+(J=1-0)] in the Pelican and Eagle Nebulae with CARMA in two array configuations (C and D). The observations were obtained in Fall 2011 and Winter 2012. To improve imaging fidelity, we combined the CARMA data on the Pelican with previous BIMA (the predecessor millimeter array to CARMA) observations covering shorter Fourier spacings. We subsequently requested CARMA Director's Discretionary Time for 6 hours of time in the CARMA E array configuration to obtain shorter Fourier spacings in the Eagle. This request was granted and the observations are scheduled for August 2012. The proposal is attached as Appendix B.

2. **CARMA Observing Proposal #2, to measure dust polarization [proxy for plane-of-sky magnetic field distribution] in Eagle Nebula**

This proposal was submitted to the CARMA TAC in Dec 2011. This proposal was also successful and was allocated 20 hours in the CARMA D array to observe $\lambda = 1$ mm polarized continuum emission from dust in the Eagle Nebula. The data were obtained in Spring 2012 and are currently being analyzed. The proposal is attached as Appendix C.

3. **CARMA Observing Proposal #3, to measure line-of-sight Magnetic field strength in Eagle Nebula via Zeeman effect.**

   As part of CARMA Observing Proposal #1, we observed two transitions of C_2H to determine its line strength (brightness) and thus suitability for a potential Zeeman measurement. Studies of the Horsehead Nebula (Gerin, Pety, & Goicoechea 2009, ASPC, 417, 165; Pety et al. 2005, A&A, 435, 885) suggested C_2H was enhanced at the edges of photo-dissociation regions, so we expected some brightness enchancement at the tips of the Eagle and Pelican pillars. Unfortunately, the lines were not detected despite fairly high sensitivity of the observations (1σ rms of 0.25 Jy/beam/channel and 0.07 Jy/beam/channel in the Eagle and Pelican, respectively) indicating unsuitability for a Zeeman measurement. The results suggest that CARMA is not currently sensitive enough to detect the expected line-of-sight magnetic field ($B \lesssim 100$ μG) via Zeeman measurements at $\lambda = 1$ mm. Therefore, CARMA Observing Proposal #3 was not produced.

   In 2013, CARMA will be equipped with $\lambda = 3$ mm full-polarization receivers. At that time, we will investigate the possibility of using 3 mm transitions of CN as a Zeeman probe. On a similar timescale, the Atacama Large Millimeter Array (ALMA) located in Chile will be equipped with full-polarization receivers as well as its full complement of 60 antennas. At that point ALMA will have higher sensitivity than any other millimeter interferometric array and we expect will be capable of successfully detecting the Zeeman effect in molecular pillar systems.

4. **Calibrated data from CARMA Proposal #1 and analysis thereof. Recommendations for density structure of experimental targets based on these astronomical data.**

   The CARMA data are fully calibrated and imaged, and we are using state-of-the art structure-finding algorithms to categorize the morphology of the dense gas in these pillar systems. The structure-finding program is being run on the HCO^+ and CS CARMA data, and ^{12}CO and ^{13}CO data from previous observations. These results will be cross-correlated to help delineate real structure from opacity effects, and allow us to determine accurate masses, sizes, and densities of all cores in the clouds. Example maps from these data are shown in Figures 1-4.

   Because we are awaiting the final CARMA observations, it is premature to give detailed recommendations for density structure of experimental targets, but it is clear from the analysis thus far that for 'clumpy targets,' a range of sizes and masses for the objects embedded in the foam would best represent the real astronomical sources. We find the cores to have mean molecular hydrogen volume densities range of $n(H_2) \sim$ few$\times 10^5$ cm^{-3}, suggesting a scaled density for clumps in the experiment in the range of 3-5 gm cm^{-3}.

5. **Reports of literature review of time variability of flux in O stars and of induced star formation in radiatively driven molecular clouds.**

   The time variability of flux of O stars in their first few hundred thousand years of life is quite difficult to assess observationally because the stars are still heavily shrouded by the dust of their natal cocoons and because of the relative rarity of O stars. The best estimate of their flux variability comes from the modeling of Palla & Stahler (1992, ApJ, 392, 667) and of Krumholz, Klein & McKee (2007, ApJ,

656, 959). These models suggest that the luminosity after the onset of hydrogen burning is a slowly rising function with time, at least until accretion ends. Because the stellar radius is also increasing during this phase, the flux $F = L/(\pi R^2)$ is actually fairly constant. In the example model shown in Figure 2, the total flux would decrease in the first 15,000 years after the onset of hydrogen burning by about 10%. There are few models which follow the flux evolution in detail after accretion stops, except for special cases such as binary systems (e.g., Song, Zhong, & Lu 2009, A&A, 504, 161). It is possible that stellar evolutionary models of massive stars (e.g., Schaller et al. 1992, A&A, 96, 269) may help us address flux variability at early times. There are additional dependencies on stellar metallicity, spectral type, and winds. We will continue to investigate this issue.

Recent work by Thompson et al. (2012, MNRAS, 421, 408) and Pomares et al (2009, A&A, 494, 987) provide evidence that triggered star formation by the expansion of H II region bubbles into molecular clouds/pillars is not uncommon. However, such triggered star formation does not typically affect the overall dynamical evolution of the pillars unless the the induced star is massive enough to create its own compact H II region (Thompson, Bradford, & Hester 2002, ApJ, 570, 749). We suggest that a NIF experiment to capture the essentials of induced star formation would be better designed separately from one intended to study the formation and evolution of pillars, perhaps as follow-on study.

6. **Reassessment of scaling parameters.**

As noted above, we find that the scaled density somewhat higher than the previous estimate of 1.3 gm cm^{-3} may be most appropriate for the clumpy target experiment. A full assessment will follow the final cloud decomposition results (mass, length, density).

Of critical importance in understanding molecular pillar evolution and dynamics is the role of the magnetic field. The astronomical observations described above allow us to obtain field morphology and strength, and help determine its relative contribution to the total energy density of the system. Furthermore, astrophysical MHD simulations show that an existing large-scale magnetic field, if it is not too strong ($\beta > 1$), can be swept into alignment parallel with a pillar during its dynamical evolution (Mackey & Lim, 2011, MNRAS, 412, 2079). This alignment occurs regardless of the initial orientation of the magnetic field. In the case of a strong external magnetic field ($\beta < 1$), the situation is reversed and the field influences the gas dynamics. Gas becomes constrained to move along field lines as does the photoablative outflow. This suggests a future experiment to test the pillar magnetic field alignment scenario. By adding initial external magnetic fields varying from $\beta << 1$ to $\beta > 1$, we could test the astrophysical simulation result.

Despite such simulations that indicate an important role for the magnetic field, scalability of the magnetic field has not been seriously addressed by investigators because the infrastructure required to add external fields to HEDLA experiments was not mature and because of lack of observational data on pillar fields. That situation is changing on both fronts and we will pursue the question of magnetic field scalability as experimental capabilities and observational results develop.

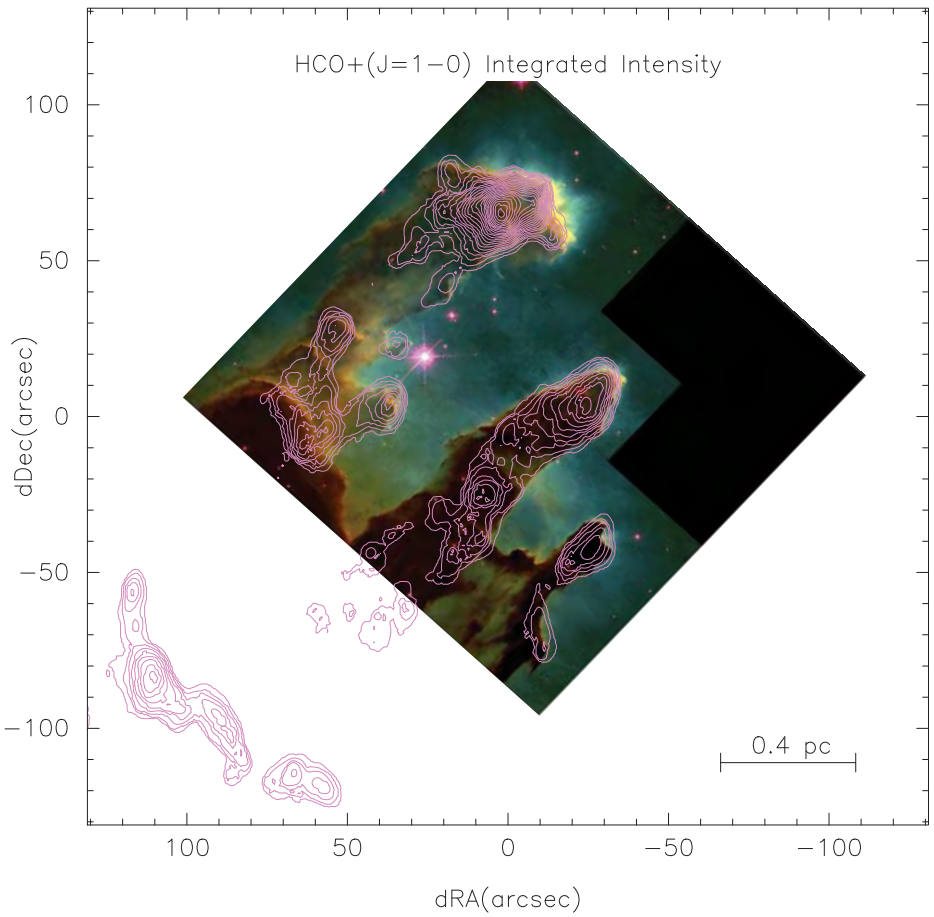

Figure 1: CARMA map of HCO^+(J=1-0) emission integrated over all velocities in the Eagle pillars (contours) overlaid on the Hubble Space Telescope optical image.

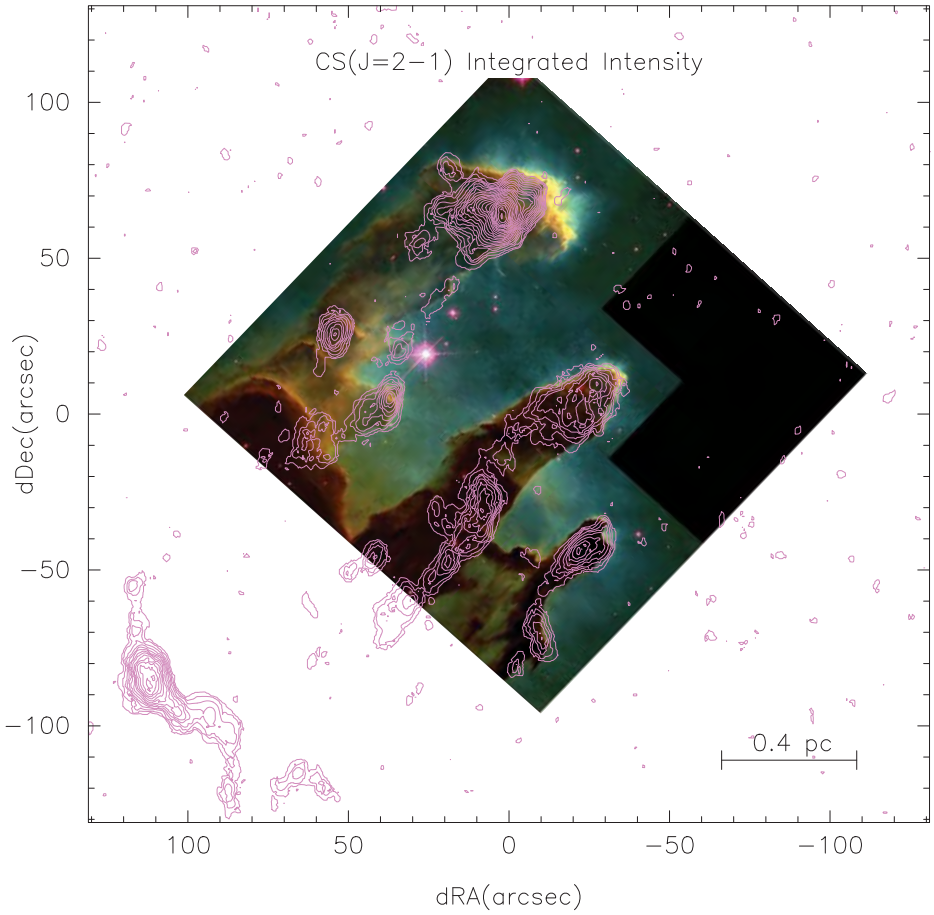

Figure 2: CARMA map of CS(J=2-1) emission integrated over all velocities in the Eagle pillars (contours) overlaid on the Hubble Space Telescope optical image.

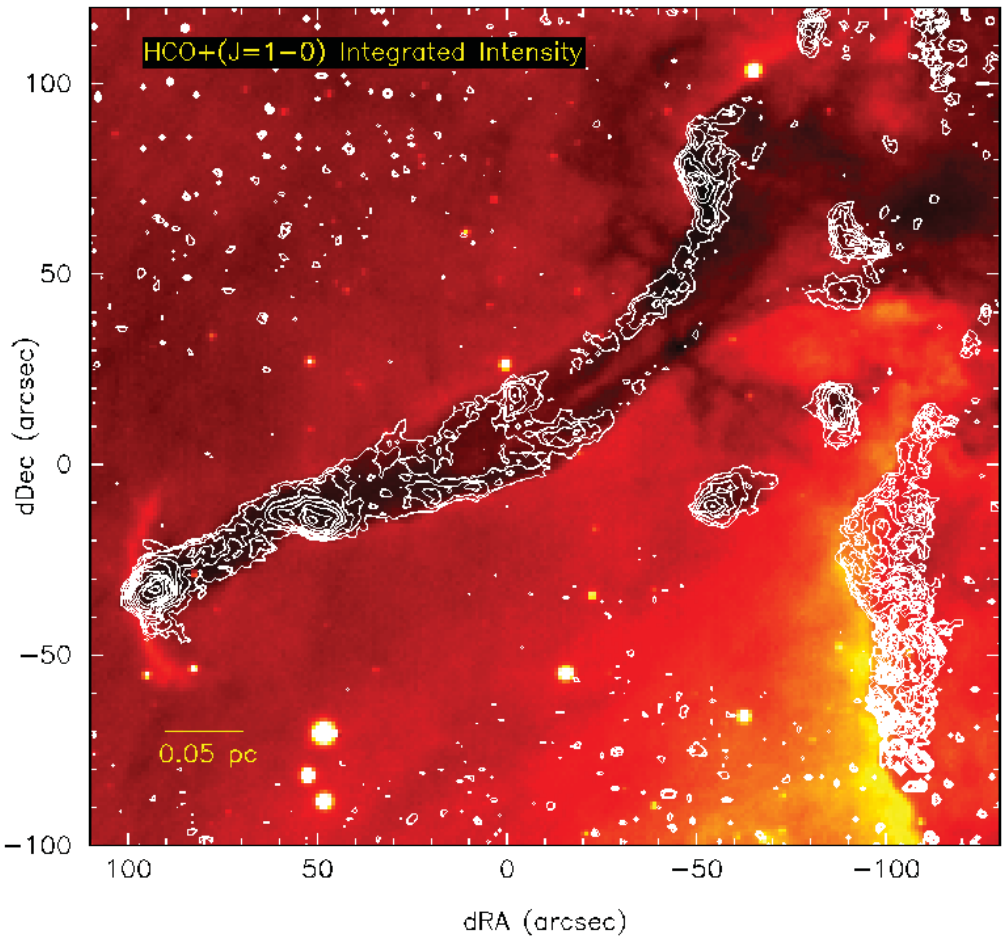

Figure 3: CARMA map of HCO^+(J=1-0) emission integrated over all velocities in the Pelican pillar (contours) overlaid on a ground-based optical image.

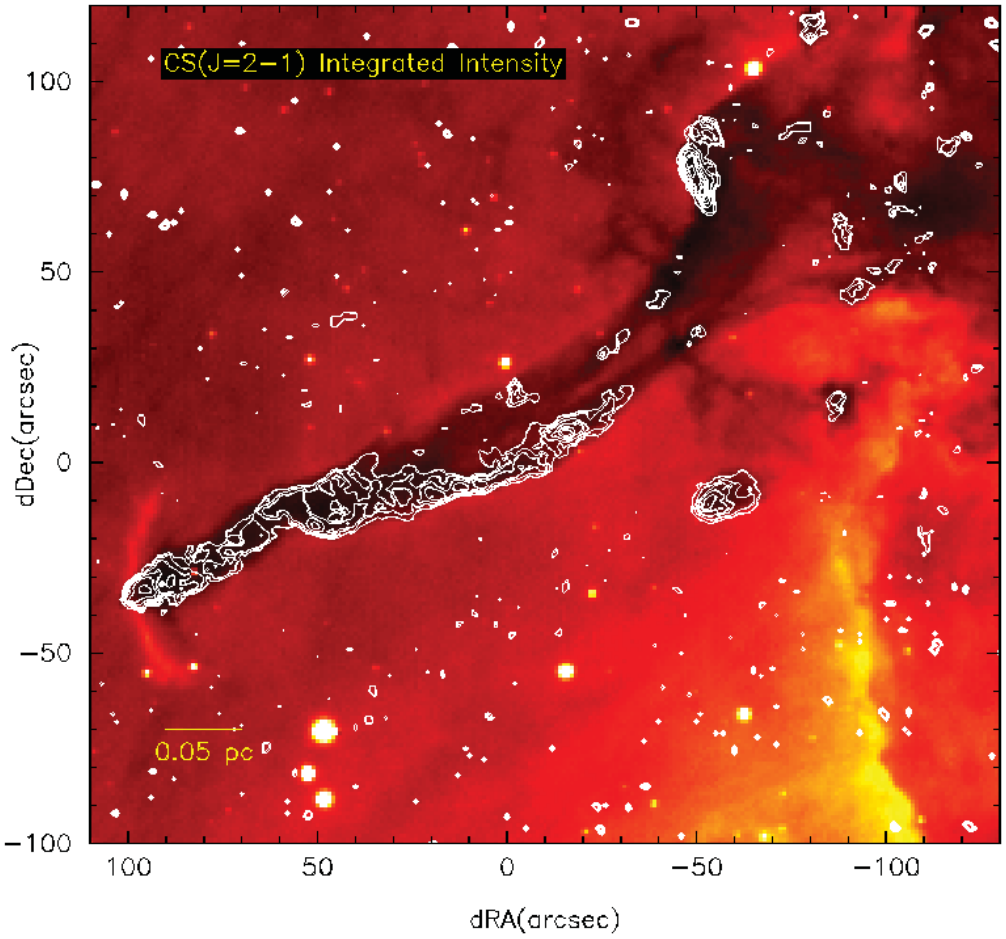

Figure 4: CARMA map of CS(J=2-1) emission intergrated over all velocities in the Pelican pillar (contours) overlaid on a ground-based optical image.

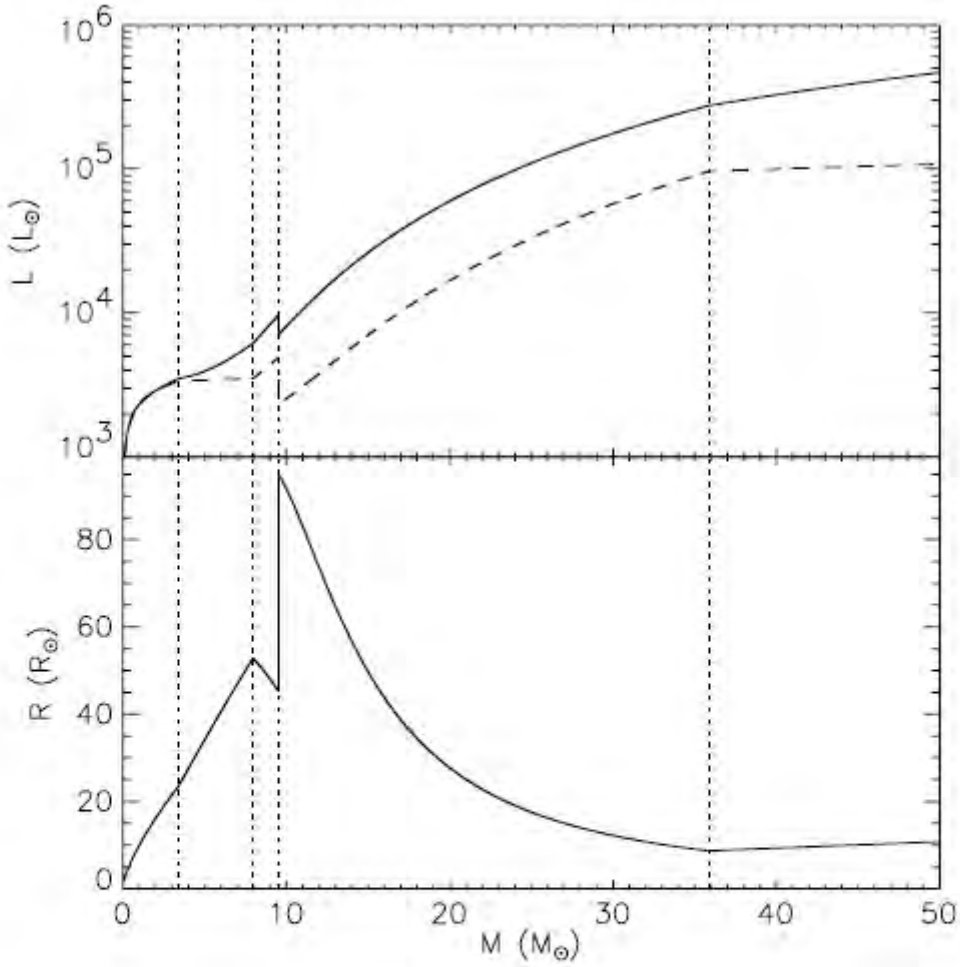

FIG. 1.—Luminosity (*top*) and radius (*bottom*) of a protostar vs. mass computed using our protostellar model with a constant accretion rate of $10^{-3}\ M_\odot\ \mathrm{yr}^{-1}$. The dashed line in the top panel is the luminosity due to accretion. The dotted vertical lines mark, from left to right, the masses at which deuterium burning starts, deuterium in the core is exhausted, convection in the envelope starts, and hydrogen burning starts.

Figure 5: Stellar luminosity and radius as a function of accreted mass from the models of Krumholz, Klein, & McKee 2007 (their Figure 1). Accreted mass is a proxy for time given the fixed accretion rate of the models.

A Poster Presented at HEDLA 2012

Characterizing the Dense Gas in the Eagle and Pelican Pillars

Erin Grand
Marc W. Pound
University of Maryland

Molecular pillars at the edge of HII regions, such as those of the Eagle and Pelican nebulae, are some of the most beautiful objects in the sky. The physics behind such pillars is determined by intense UV radiation from nearby bright young stars. The radiation causes different physical processes to come into play: hydrodynamic instability, photoionization, ablation, recombination, molecular heating and cooling. This intense environment is amenable to coordinated study with observations, theory and modeling, and HEDLA experiments. Before fielding an experiment, we need well characterized cloud properties, which is the focus of this poster.

Importance

Pillars like those of the Eagle and Pelican are examples of a phenomenon that is commonly seen wherever molecular clouds are situated near O stars: large "fingers" of dense gas and dust that point back at the highly energetic young stars. Proposed formation mechanisms for such pillars generally fall into two broad categories: i) instabilities at the boundary between the cloud and the ionized region which grow with time (e.g. [1,2,3,4]) and ii) pre-existing density enhancements (clumps) which locally retard the ionization front, creating cometary globules.[5,6]

By studying the underlying mass, density, size, and velocity distributions of the gas in these structures, we can examine the relative roles each of these mechanisms play in pillar formation.

Observing with CARMA

The Combined Array for Research in Millimeter-wave Astronomy (CARMA) is a interferometric array made up of 23 radio antennas, located at 2195 m at Cedar Flat in the Inyo Mountains of California. Interferometers like CARMA measure the Fourier Transform of the sky brightness distribution, called the visibility function. As the Earth rotates, antenna pairs trace out ellipses in the Fourier (u,v) domain, sampling different spatial frequencies of the source structure. Any smooth component of the structure is "resolved out" because the shortest antenna separation is non-zero. For the Eagle and Pelican pillars, the lack of short-spacing data is less of a concern because the pillar substructure is small compared to the primary beam field-of-view (~60").

We have obtained new mm-wavelength observations with CARMA to look at the underlying structure of dense gas in these objects. We mapped the spectral line emission from molecules which trace high-density gas, $n(H_2) > 10^4\,cm^{-3}$, specifically CS, HCO+, HCN, and N2H+.

What about Magnetic Fields?

The strength and orientation of the magnetic field threading the pillars can strongly affect their formation and evolution.[7,8] With upcoming CARMA observations of polarized emission from dust in the Eagle, we will be able to determine the B-field orientation for the first time ever in any molecular pillar. Furthermore, using the simulations of Mackey & Lim we can not only determine the most probable three-dimensional B-field morphology, but estimate its strength without recourse to observationally expensive Zeeman measurements. (See Friday talk by J. Mackey).

Science Use on NIF

We have recently been granted HEDLP funding to develop a collimated long duration drive, leveraging and refining the existing NIF Radiation Transport platform. We will use the new drive to generate long-duration highly directional irradiation, ablation, and compression of scaled targets; investigate novel dynamics of photoionization fronts molecular pillars irradiated by luminous O-type stars; and quantitatively compare the results to our CARMA observations. (See poster by J. Kane).

Future Work

We will analyze the data from the other spectral lines to better determine clump properties from multiple maps. From these data, we will derive the scaling parameters for these systems required for designing the NIF experiment. We also need to find a fractional abundance of HCO+ more appropriate to the extinction and ionization state of these systems, allowing more accurate mass estimates. A larger fractional HCO+ abundance would push the clumps toward virialization. We may obtain shorter spacing data for the Eagle which could marginally increase the masses and sizes of the larger clumps.

Pelican Nebula

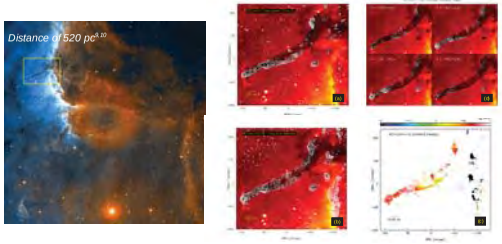

Figure 1a-b: Integrated emission over all velocities for CS and HCO+ respectively.
Figure 1c: Examples of individual velocity channel maps with a resolution of 0.33 km/s shown for HCO+.
Figure 1d: Velocity centroid map for HCO+ showing the overall velocity distribution.

Eagle Nebula

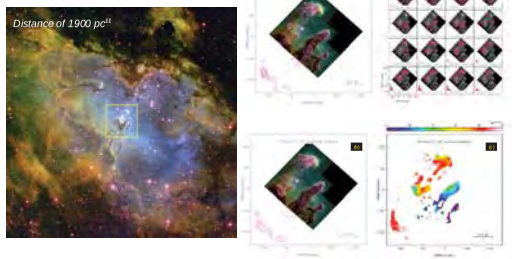

Figure 2a-b: Integrated emission over all velocities for CS and HCO+ respectively.
Figure 2c: Examples of individual velocity channel maps with a resolution of 0.33 km/s shown for HCO+.
Figure 2d: Velocity centroid map for HCO+ showing the overall velocity distribution.

Cloud Morphology

From the detailed maps of molecular emission we can derive physical properties such as mass, density, size, and velocity distributions within the clouds. We can clearly see the large heads and pillar forms of the nebulae as well as substructure within them. Given our high resolution, it is evident that the molecular emission mirrors the features seen in the visible images extremely well, so we are confident the interferometer is not missing significant structure.

The morphology of CS and HCO+ agree, as shown in the integrated intensity and channel maps (Figure 1 and Figure 2). Differences could be caused by chemistry within the clouds. For the Pelican, u-v sampling differences may also contribute.

By measuring the gas radial velocities, we observe how the velocities vary over the pillar. Earlier CO maps of the Eagle[12] found large scale velocity gradients along the length of the pillars. Our higher resolution observations confirm that result but also reveal a rich and complex velocity field (Figure 2d). Like the Eagle, the Pelican has an overall velocity gradient between head and base, dV/dR ~3 km/s/pc. However, the Pelican's velocity field appears less complex than that of the Eagle, perhaps reflecting its less intense environment.

Clump Properties

Using well-established structure-finding algorithms[12], we derive the mass, size, and velocity distributions of dense clumps in the pillars. There are two commonly used methods to estimate mass. First, we can look at the line width, ΔV, and size of the clump, R, to estimate a virial mass, given by $M_{vir} \approx \Delta V\, R^2$. Secondly, we can use the total flux in each clump to calculate a H_2 luminosity mass. We do this by assuming a conversion factor from the brightness of molecular emission to H_2 column density which is dependent on the dipole moment and fractional abundance of the molecule. In Figure 3, for each clump, the two mass estimates are plotted against each other. If the clumps are virialized, then we would expect them to follow a $\Delta V \sim R^{0.5}$ distribution. As shown in Figure 3, this is not the case for either nebula, implying the clumps are not virialized. We also find the average mass, line width, and size of the Eagle clumps to be larger than those of the Pelican.

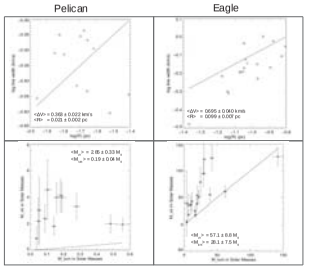

Figure 3 (top): Line width vs. radius for the clumps found in the Eagle and Pelican, derived from the HCO+ data. The solid line corresponds to $\Delta V \sim R^{0.5}$ expected for virialization.
Figure 3 (bottom): Virial mass vs. luminosity mass for the clumps found in the Eagle and Pelican, derived from the HCO+ data. The solid line corresponds to $M_{lum} = M_{vir}$.

Acknowledgments

This work was supported by NIF Concept Development award B595751 from DOE/LLNL, "Dynamics of the Eagle Nebula."

Support for CARMA construction was derived from the states of Maryland, California, and Illinois. Ongoing CARMA development and operations are supported by the National Science Foundation under a cooperative agreement, and by the CARMA partner universities.

References

1. Spitzer 1954, ApJ, 120, 1
2. Fieman 1954, ApJ, 120, 18
3. Williams et al. 2001, MNRAS, 327, 788
4. Mizuta et al. 2005, ApJ, 647, 1151
5. Reipurth 1983, A&A, 117, 183
6. Bertoldi & McKee 1990, ApJ, 354, 529
7. Henney et al. 2009, MNRAS, 398, 157
8. Mackey & Lim 2011, MNRAS, 412, 2079
9. Laugalys et al. 2006, BalticAstron, 15, 483
10. Straizys et al. 1989, Baltic Astron, 8, 335
11. Hillenbrand et al. 1995, AJ, 106, 1906
12. Pound 1998, ApJ,493L, 113
13. Rosolowsky & Leroy 2008, PASP, 118, 590

B CARMA Dense Gas Proposal

Combined Array for Research in Millimeter-wave Astronomy

Observing Proposal Cover Sheet

Proposal Number

c0770

General Proposal Information

Title		Date	TOO/Time Critical	Key Project
Towards a Laboratory Analog of the Eagle Nebula		2011-04-26	–	–
Scientific Category	**1cm Project**	**3mm Project**	**1mm Project**	**Level of Help Required**
Chemistry / Interstellar Medium	–	X	–	None

Authors

#	Name	E-mail	Phone	Institution	Thesis	Grad
PI	Marc Pound	mpound@umd.edu	301.405.1520	UMD	–	–
2	Amy Cooper	cooper64@llnl.gov	925.423.8942	Lawrence Livermore National Lab	–	–
3	Jave Kane	kane7@llnl.gov	925.424.5805	Lawrence Livermore National Lab	–	–
4	Bruce Remington	remington2@llnl.gov	925.423.2712	Lawrence Livermore National Lab	–	–
5	Dmitiri Ryutov	ryutov1@llnl.gov	925.424.2468	Lawrence Livermore National Lab	–	–
6	Vladimir Smalyuk	smalyuk2@llnl.gov	925.422.9832	Lawrence Livermore National Lab	–	–

Advisor must send a supporting letter if Thesis is checked. See Instructions.

Abstract

Sometimes the most beautiful things are the hardest to understand. Pillars like those of the Eagle Nebula form at the boundary between some of the hottest (10,000K) and coldest (10K) gas in the Galaxy. Many physical processes come into play in the birth and growth of such gaseous pillars: hydrodynamic instability, photoionization, ablation, recombination, molecular heating and cooling, and probably magnetic fields. High-quality astronomical observations, quantitative numerical simulations, and scaled laser experiments provide a powerful combination for understanding their formation and evolution.

To guide our design of a scaled astrophysics experiment on the world's largest laser, the National Ignition Facility (NIF), to understand pillar formation, we propose CARMA observations to measure the high density structure in two sources: the Eagle and the Pelican. These pillars appear to be at opposite extremes of density distribution in molecular pillars, with the Eagle being very clumpy and the Pelican appearing smooth. Understanding their density structure over a wide range of spatial scales is crucial for designing a NIF target.

We also propose to assess the feasibility of using a new molecule to measure the Zeeman effect in photo-dissociation regions. The magnetic field may play an important role in resisting the ablative pressure from the O-star ionizing photons.

Source Information

#	Source	RA	DEC	Freq	A	B	C	D	E	SL	# Fields	Species	Imag/SNR	Flex.HA
1	Eagle	18:19	-13:50	98	0	0	10.5	10.5	5.25	0	37	CS(2-1)	Imaging	–
2	Pelican	20:51	44:26	98	0	0	8	8	8	0	19	CS(2-1)	Imaging	–

Total Hours: 50.25

Special Requirements

Although the PI is at UMD, this proposal is part of large experimental collaboration with mostly external co-Is. We therefore request that be 50% charged to UMD time and 50% to visitor time.

Note we have been awarded FY12 funding to obtain and analyze the observations proposed herein.

Status of Prior CARMA Observations

VeLLOs Survey: All previous observations calibrated, reduced, and mapped. Initial results presented at 2011 CARMA Science Symposium. Final stage of survey being conducted now.

NGC1333 CARMA-23 mosaic: Data completely calibrated and reduced. Working on techniques of combining interferometric and

singledish data.

Scientific Justification

The Eagle Nebula, with its majestic pillars, is one of the most recognized objects in the sky. The underlying dynamics of the Eagle Nebula are driven by the intense UV radiation from nearby young stars, which causes photo-dissociation and ionization of the cloud surface layers. The resulting ablation pressure compresses the cloud and generates complex, radiative hydrodynamic evolution, while the interior remains dense and cold because of strong radiative cooling.

Do these pillars form as an effect of radiative hydrodynamic instabilities or as a result of pre-existing enhanced-density clumps in the cloud, or by some entirely different process? Fundamental theory alone has not conclusively answered these questions due to the complexity of the nonlinear radiation hydrodynamics at the heart of the Eagle Nebula [1].

While the Eagle Pillars are a particularly spectacular example of radiatively driven molecular clouds (RDMCs), such structures are commonly seen wherever molecular clouds are situated near O stars. Others examples include the Pelican Nebula and the Horsehead [2,3]. Because pillars are common, determining the details of how they form and dissipate is important for understanding molecular cloud evolution after the first stars form.

Our team has been at the forefront of an effort to develop scaled experiments on the National Ignition Facility (NIF) where intense radiation can flow long enough to drive hydrodynamics into the deep nonlinear regime, as in the Eagle pillars. With a scaled experimental test bed, we can investigate the Eagle Nebula dynamics in all aspects: combining astronomical observations, fundamental theory, radiation-hydrodynamics simulations, and scaled validation experiments. This would be an unprecedented achievement and a new paradigm in astrophysics research.

We have made significant progress in both theory and radiative hydrodynamic simulations, grounding both in the physical parameters that are deduced from existing observations, and comparing the simulations to the observations [1,4,5,6]. **This project has now been selected to begin detailed planning for laser time, starting in FY12 on NIF, the world's largest laser, as part of the *Science Use on NIF* program.**

High-energy density laboratory experiments must be designed to scale appropriately the physical properties of the astrophysical object (see, e.g. [7,8]). In our NIF experiment, a laser will be used to heat a small gold cylinder, called a hohlraum, causing it to give off UV and X-ray photons which irradiate a target, analagous to an O-star irradiating a molecular cloud (Figure 1). Crucial to our target design are two questions which can be answered by CARMA observations:

1. *What are the appropriate clump number, density, and size distributions? How do these differ from cloud to cloud?* In both optical/IR dust and radio molecular tracers, some RDMCs look clumpy (Eagle), while other appear smooth (Pelican), and some are in-between (Horsehead). The density distribution in these structures is directly relevant to the material response to ablative pressure from the ionization front. NIF experimental targets can be fabricated with variations in density and surface shape that may seed growth of cometary structures and Rayleigh-Taylor and Richtmyer-Meshkov instabilities, for example using high density inclusions having various sizes and aspect ratios **We propose CARMA observations of high density tracer molecules in the Eagle and Pelican sources to directly address this question.**

2. *How important are magnetic fields for clouds support?* It is not yet known if magnetic fields

are dynamically important in RDMCs. Are clouds threaded by magnetic fields which are coherent on scales comparable to the cloud size or are they tangled on much smaller scales ("magnetostatic support" [4])? This can be addressed via CARMA observations to measure the Zeeman effect and dust polarization. If we find magnetic fields are dynamically important, we will choose target materials with equations of state that approximate magnetic support.

Measurement of the Zeeman effect in dense molecular clouds has typically been attempted with CN(1-0), which has a large Zeeman splitting of its hyperfine components ($Z = 2.2$ Hz/μG; [9]). However, its low abundance and low temperature in cold cloud cores combine to require long integration time for sufficient sensitivity. However, another molecule, C_2H, has equally large Zeeman splitting ($Z = 2.6$ Hz/μG; [10]) and may be ideally suited for determining magnetic fields in RDMCs. While C_2H is depleted in dense cores, its emission is comparatively bright at the *edges* of RDMCs, with an abundance up to 10× higher than dense-core CN [11,12]. **We propose to measure the brightness of C_2H(1-0) emission to assess the feasibility of a future CARMA proposal to measure magnetic fields in these clouds using C_2H(3-2).**

Technical Justification

The correlator setup for all observations will be 6x8 MHz/3BIT bands plus 2x500 MHz/3BIT bands. The 8MHz bands will be placed on the CS(2-1), N_2H+(1-0), HCO+(1-0), HCN(1-0), and the 3 transitions of C_2H(1-0) with large Zeeman coefficients. The 500 MHz bands will be used for calibration and as an alternate measure of total mass via dust continuum emission. We will average the 8 MHz channels to 0.2 km/s. (For comparison with radiative hydrodynamic numerical simulations, high spectral resolution is necessary).

Our Pelican data from the BIMA array show a mean flux density of HCO+(1-0) per 0.33 km/s channel of $\sim$ 300 mJy/beam in the BIMA 15″ beam (Figure 2). The cloud structure is clearly unresolved in this beam, so we would expect the D- and C-array average brightness to be somewhat higher. A mosaic of 20 fields at the Nyquist sampling of the 98 GHz CS beam will cover the Pelican pillar and part of the parent molecular cloud at the base of the pillar.

For the Eagle, JCMT observations show an HCN(1-0) brightness temperature of 2K in a 44″ beam and HCO+(4-3) brightness of 6K in a 14″ beam [13]. Our BIMA CO(1-0) observations (Figure 2) show clumping on size scales as small as the beam ($\sim$ 5″) and HST image shows structure even smaller. A standard hex-37 mosaic will cover the same area as the BIMA observations.

In PdBI observations of the Horsehead, C_2H(1-0) has brightness temperature 1-3 K in a 6″ beam ($\sim$ 300 mJy/beam) [11]. Because the dominant physical and chemical processes are similar, we expect comparable flux density from the Eagle and Pelican.

For both sources, we require a resolution of a few arcseconds to determine clump parameters over a range of size scales. To reach a combined 1σ RMS of $\lesssim$ 100 mJy/beam in and 0.2 km/s channel, we request 1 E, 2 D, and 2 C configurations tracks for Eagle, and 1 track each of E, D, and C for Pelican, for a total of 50 hours and resolution of 2–3″. (from CARMA RMS Calculator).

References: [1] Mizuta, Kane, Pound, Remington, Ryutov, & Takabe 2006, ApJ, 647, 1151; [2] Pound, Reipurth, & Bally, 2003, AJ, 125, 2108; [3] Habart, Abergel, Walmsley, Teyssier, & Pety 2005, A&A, 437, 177; [4] Ryutov, Kane, Mizuta, Pound & Remington 2004, AIPC, 703, 415 [5] Ryutov, Kane, Mizuta, Pound & Remington 2007, Ap&SS, 298, 307; [6] Pound, Kane, Remington, Ryutov, Mizuta, & Takabe, 2005, Ap&SS, 298, 177; [7] Ryutov, Drake, Kane, Liang, Remington, Wood-Vasey, 1999, ApJ, 518, 821; [8] Ryutov, Drake, & Remington 2000, ApJS, 127, 465; [9] Crutcher, Troland, Lazareff, & Kazes, 1996, ApJ, 456, 217; [10] Bel & Leroy 1998, A&A, 335, 1025; [11] Pety, Teyssier, Fosse, Gerin, Roueff, Abergel, Habart, & Cernicharo 2005, A&A, 435, 885; [12] Hily-Blant, Walmsley, Pineau Des Forets, & Flower 2008, A&A, 480, 5; [13] White et al. 1999, A&A, 342, 233; [14] Pound, 1998, ApJ, 493, 113

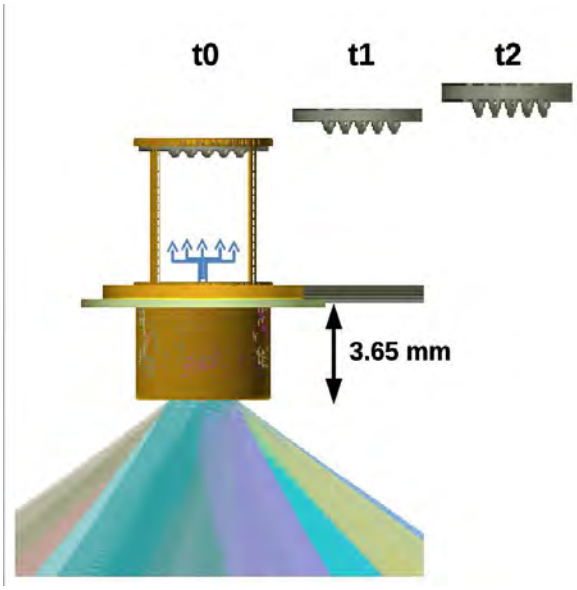

Fig. 1.— Proposed Eagle Nebula experiment target to examine pillars as instability growth. At time t0, a gold hohlraum is heated from one side with 80 laser beams (shown here entering from below), creating a radiation source of 100-150 eV for 20 ns. This radiation heats and accelerates a machined, rippled foam (t1), which accelerates the bulk surface via the rocket effect and causes Rayleigh-Taylor growth of the initial perturbations (t2).

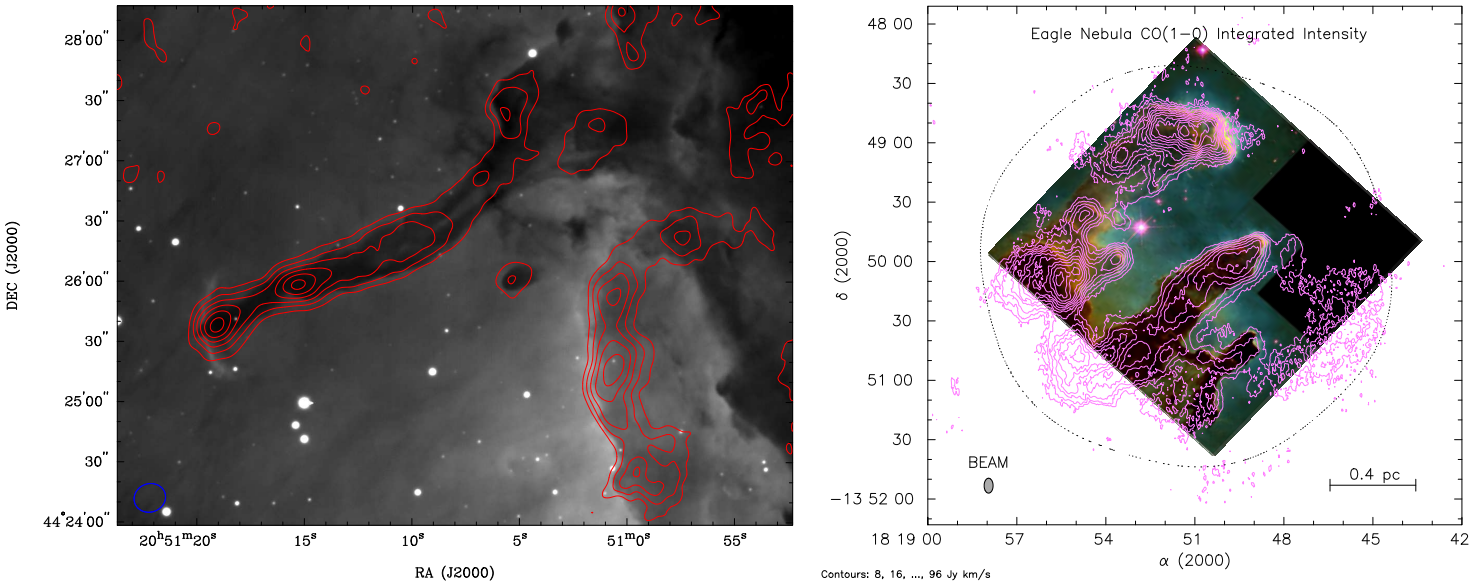

Fig. 2.— *left)* HCO+(1-0) map of the Pelican from BIMA (unpublished), overlaid on an optical image. The BIMA resolution is $15'' \times 14''$. Contours are 0.8 Jy km/s (3 σ). *right)* CO(1-0) map of the Eagle from BIMA [14], overlaid on the HST image. The BIMA resolution is $7'' \times 4''$. Contours are 8,16,...,96 Jy km/s (many σ).

C CARMA Dust Polarization Proposal

Combined Array for Research in Millimeter-wave Astronomy

Observing Proposal Cover Sheet

Proposal Number

c0902

2012a

General Proposal Information

Title				Scientific Category		
Determining the Magnetic Field Morphology in the Eagle Nebula Pillars				Chemistry / Interstellar Medium		
Date	**Key Project**	**TOO/Time Critical**	**Level of Help Required**	**1cm Project**	**3mm Project**	**1mm Project**
2011-12-05	–	–	Consultation	–	–	X

Authors

#	Name	E-mail	Phone	Institution	Thesis	Grad
PI	Marc Pound	mpound@umd.edu	301 405 1520	UMD	–	–
2	Jonathan Mackey	jmackey@astro.uni-bonn.de	+49-228-733783	Argelander Institut fur Astronomie/Humboldt Fellow	–	–

Advisor must send a supporting letter if Thesis is checked. See Instructions.

Abstract

We propose measure the magnetic field morphology in the Eagle Nebula pillars with 1.3mm continuum dust polarization in CARMA's Full-Stokes mode. We will couple these new measurements with existing interferometric measurements of CO, CS, HCN, HCO+, and N2H+ to compare with our simulations of pillar formation in the presence of magnetic fields. These simulations provide projected column density maps, position-velocity diagrams, and plane-of-sky magnetic field maps for a variety of field configurations and strengths. With such analysis we can not only determine the most probable three-dimensional magnetic field morphology, but estimate its strength without recourse to observationally expensive Zeeman measurements. This would be the first time magnetic field measurements have been made in any molecular pillar system.

Source Information

#	Source	RA	DEC	Freq	C	D	E	SH	SL	Type	# Fields	Species	Imag/SNR	Flex.HA
1	M16	18:18	-13:50	225	0	20	0	0	0	FP	13	continuum	Imaging	–
Total Hours: 20.0														

Special Requirements

While this project might be "safer" to do in the lower resolution E-array, the poor summer 1mm weather would doom it to failure, especially since the source is up during the daytime in summer. If there is to be a winter E-array, we would be amenable to a swap for an equal number of unshadowed hours in that configuration.

Status of Prior CARMA Observations

Mackey - None

Pound - c0770 data being reduced and analyzed by UMD grad student Erin Grand

Scientific Justification

Pillars like those of the Eagle Nebula form at the boundary between some of the hottest (10000K) and coldest (10K) gas in the Galaxy. Many physical processes come into play in the birth and growth of such gaseous pillars: hydrodynamic instability, photoionization, ablation, recombination, molecular heating and cooling, and magnetic fields. While the Eagle Nebula pillars are perhaps the most spectacular example of this phenomenon (Hester et al. (1996)), they are not the only one. Such pillars are seen all over the sky, wherever young, hot stars are bursting out of their natal cocoons.

The formation mechanism of pillars at the borders of H II regions is still not fully understood, and hence the timescale over which they form and their lifetimes are also not well constrained. 2D and 3D radiation-hydrodynamical numerical simulations have shown that a number of processes can form such structures: ionization front instabilities (e.g. García-Segura & Franco 1996; Whalen & Norman 2008), shadowing due to pre-existing non-linear inhomogoneities (e.g. Kessel-Deynet & Burkert 2003; Pound et al. 2007; Mackey & Lim 2010), and more generally the pressure-driven expansion of H II regions in a turbulent medium (Mellema et al. 2006; Gritschneder et al. 2010) in which a combination of the previous two mechanisms can be acting. Recently the effects of magnetic fields on this process have been studied. It has been shown that the strength and orientation of the B-field can strongly affect the formation and evolution of pillars from radiation-driven-implosion of a single clump (Henney et al. 2009), multiple clumps (Mackey & Lim 2011) and in a turbulent medium (Arthur et al. 2011). Effects are seen both in the ionized and neutral gas dynamics and morphology, as well as the evolution of the B-field configuration within the pillar.

Mackey & Lim (2011) modelled the photoionization of dense magnetized gas clumps due to a point source of radiation with 3D simulations. From these calculations maps of the neutral gas column density and plane-of-sky B-field orientation are shown in Fig. 1 for simulations with an initially weak field of $B = 18\,\mu$G (above) and a rather strong field of $B = 160\,\mu$G (below), after 300 kyr (left) and 400 kyr (right) of evolution. For weak and medium field strengths an initially perpendicular field is swept into alignment with the pillar during its dynamical evolution, whereas a strong field remains in its initial configuration. These results showed that magnetic field strengths in star-forming regions can in principle be significantly constrained by the morphology of pillars coupled with measurements of the B-field orientation. Near infrared polarimetry by Sugitani et al. (2007) indicates that the B-field within the Eagle Nebula pillars may be aligned with the pillar and misaligned with the larger scale field in th H II region, suggesting that the B-field is significantly weaker than in the $160\,\mu$G strong field simulations. However, polarized emission from dust is a better tracer of the field within the pillars because it has uniform coverage over the whole pillar rather than 'pencil-beams' through regions of low extinction.

Maps of CO J=1-0 and J=2-1 emission from the Eagle pillars made with BIMA (Fig. 2, Pound 1998) show bright, large, elongated cores with clumpy substructure and large velocity gradients along their length. Continuum maps obtained with JCMT show many embedded submillimeter continuum cores that correspond to the CO cores, the most intense of which are located at the tips of the pillars, and with temperatures of ∼20 K (White et al. 1999). The brightest of these continuum cores is in Pillar I, with a peak brightness of 475 mJy/beam at 1.3mm. Recent CARMA D-array observations (project c0770) of CS, HCN, HCO+, and N2H+ reveal several high density

cores within the pillars. Infrared observations with ISOCAM and Spitzer show the colder cores are wrapped in hot outer shells with T=250-300K (Pilbratt et al. 1998) and contain a few YSOs whose formation has perhaps been triggered by the nearby young stellar cluster NGC 6611 (Indebetouw et al. 2007).

While the Eagle pillars are the most well-studied molecular pillar system, we still have almost no knowledge of the strength or orientation of the embedded magnetic field. Indeed, no unambiguous magnetic field measurements exist for *any* pillars anywhere. Thus it is unclear if the magnetic field is dynamically important in the formation and evolution of these structures. **We propose here to use CARMA's new Full-Stokes capability to measure for the first time the magnetic field direction in a molecular pillar via 1.3mm dust polarization**. The high spatial resolution of CARMA will provide dozens of independent polarization angle measurements with an uncertainty of <10%.

The simulations of Mackey & Lim (2011) provide projected column density maps, position-velocity diagrams, and plane-of-sky B-field maps for a variety of B-field configurations and strengths. This enables a detailed comparison with the BIMA CO observations, the CARMA high-density spectral line data, the CARMA 1.3mm dust polarization measurements we propose here, and the larger scale, H II region starlight polarization measurements of Sugitani et al. (2007). The simulation code has since been improved by J. Mackey, with more realistic thermal physics in the neutral gas, so it will be possible to make further simulations tailored specifically to model the data obtained from CARMA. **With such analysis we can not only determine the most probable three-dimensional B-field morphology, but estimate its strength without recourse to observationally expensive Zeeman measurements.** We can further apply the modified Chandrasekhar & Fermi (1953) technique discussed by Padoan et al. (2001) to the CARMA high-density spectral line data to make an independent estimate the B-field strength.

Technical Justification

We will concentrate on the head of Pillar I, which is the brightest and densest location in the Eagle Pillars. We will use the CARMA D array configuration in Full-Stokes mode with all bands set to 500MHz/3BIT for a total continuum bandwidth of 4 GHz. At 225 GHz, the spatial resolution will be 3″ or about 5700AU at the distance of the Eagle. The 1.3mm continuum flux density from White et al. (1999) is between 150 and 475 mJy/beam. Assuming a polarization of 3% gives an expected polarized signal of 5 and 14 mJy. With 13 fields to cover the head of Pillar I (Fig. 2), 20 hours will give an expected rms of 1.2 mJy/beam (CARMA Sensitivity calculator). We request some technical assistance in setting up the observing script calibration requirements, such as measuring the phase difference between the L and R receivers ("xyphase").

REFERENCES

Arthur, S. J., Henney, W. J., Mellema, G., de Colle, F., & Vázquez-Semadeni, E. 2011, MNRAS, 414, 1747
Chandrasekhar, S., & Fermi, E. 1953, ApJ, 118, 113
García-Segura, G., & Franco, J. 1996, ApJ, 469, 171
Gritschneder, M., Burkert, A., Naab, T., & Walch, S. 2010, ApJ, 723, 971
Henney, W. J., Arthur, S. J., de Colle, F., & Mellema, G. 2009, MNRAS, 398, 157
Hester, J. J., Scowen, P. A., Sankrit, R., et al. 1996, AJ, 111, 2349
Indebetouw, R., Robitaille, T. P., Whitney, B. A., et al. 2007, ApJ, 666, 321
Kessel-Deynet, O., & Burkert, A. 2003, MNRAS, 338, 545
Mackey, J., & Lim, A. J. 2010, MNRAS, 403, 714
—. 2011, MNRAS, 412, 2079
Mellema, G., Arthur, S., Henney, W., Iliev, I., & Shapiro, P. 2006, ApJ, 647, 397
Padoan, P., Goodman, A., Draine, B. T., et al. 2001, ApJ, 559, 1005
Pilbratt, G. L., Altieri, B., Blommaert, J. A. D. L., et al. 1998, A&A, 333, L9
Pound, M. W. 1998, ApJ, 493, L113
Pound, M. W., Kane, J. O., Ryutov, D. D., Remington, B. A., & Mizuta, A. 2007, Ap&SS, 307, 187
Sugitani, K., et al. 2007, PASJ, 59, 507
Whalen, D., & Norman, M. 2008, ApJ, 672, 287
White, G. J., Nelson, R. P., Holland, W. S., et al. 1999, A&A, 342, 233

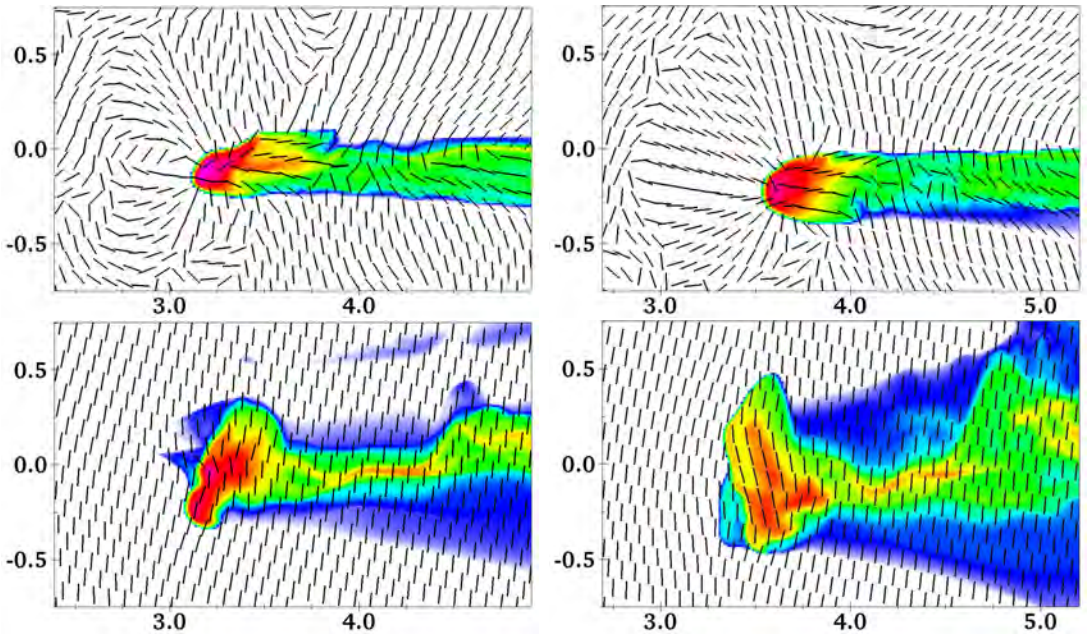

Fig. 1.— Projections through 3D dynamical simulations of photoionized pillars (Mackey & Lim 2011) threaded by weak (top) and strong (bottom) magnetic fields, shown at times 300 kyr (left) and 400 kyr (right). Neutral hydrogen column density is plotted on a logarithmic scale (3×10^{19} to 3×10^{23} cm^{-2}). Projected magnetic field orientation in the plane of the sky is indicated by the black lines. Positions are shown in parsecs relative to the ionizing radiation source which is off the computational domain to the left.

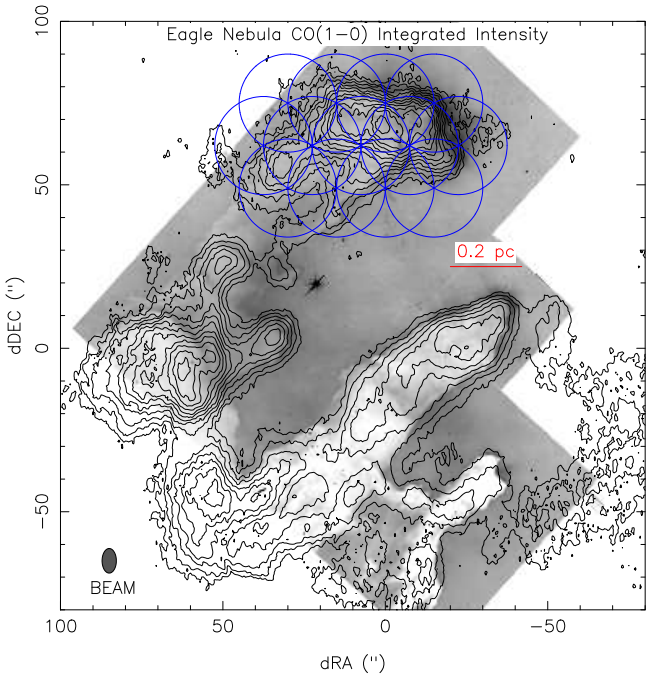

Fig. 2.— BIMA CO(1-0) integrated intensity overlaid on HST image of the Eagle Pillars (contours 8,16,...,96 Jy km/s, resolution $7'' \times 4''$). The proposed CARMA 1.3mm dust polarization mosaic is shown in blue circles.